f_x fall permanently below e^{-1}. The 4–5-fold periodicity in f_x persists beyond $x = 75$, where $f_x = 0.046$; at $x = 200$, $f_x = 0.0003$. The longer range directional correlations implicit in f_x for the ATC model compared to the CTC model are an obvious reflection of the more constrained parabolic energy surfaces required to fit the $\langle s_x^2\rangle_0/xL^2$ vs. x data for ATC. Comparison of the calculated values of a_x and f_x for CTC and ATC shows clearly how these two parameters can provide complementary information about polymer directional correlations.

One other plausible model for ATC was investigated. It is conceivable that the stiff and flexible states of ATC occupy distinctly different regions of the residue conformation space. For example, the long-range interactions of phenylcarbamate substituent groups postulated to stabilize the stiff state may occur only when the substituent group alignment is that which occurs in the fully extended conformations characteristic of the secondary minimum on the maltose energy map. Transition from the flexible to the stiff state with increasing x may then involve a significant change in residue conformation, e.g., from the primary to the secondary minimum. We have, in fact, investigated the opposite situation, taking $\phi_0,\psi_0 = -20,-170°$ for the flexible state and $\phi_0,\psi_0 = -50,-40°$ for the stiff state. The motivation for this choice is that since the stiff state, thus chosen, is also the one characterized by less extended chain conformations, the slow transition of $\langle s_x^2\rangle_0/xL^2$ from rodlike to Gaussian behavior in ATC might be more effectively modeled. With $s = 1.00$ and $\sigma = 3.0 \times 10^{-5}$ and for various choices of K_s and K_f, no adequate fit to the experimental data could be achieved. When the data were fit in the asymptotic region, curves resembling that in Figure 12 were always observed. We have no doubt that the data could be fit with models of this type, provided a small enough value of σ were chosen, but we currently have no justification for this elaboration of the model relative to the model used to produce the best fit shown in Figure 13. It should be observed, however, that the very small σ value required to fit the ATC data might result in part from a large interfacial free energy associated with the junction zones between chain segments in two quite different conformational states.

Acknowledgment. The work reported here has been supported by NSF Grant PCM 79-23041. This work was begun when D.A.B. was a visitor at the Institut für Makromolekulare Chemie, Universität Freiburg, under the sponsorship of the John Simon Guggenheim Memorial Foundation. We also acknowledge the award to B.H. of an ACS Division of Polymer Chemistry Summer Scholarship sponsored by the Proctor and Gamble Co., summer 1980.

References and Notes

(1) Burchard, W. *Z. Phys. Chem. (Frankfurt/Main)* **1964**, *42*, 293.
(2) Burchard, W. *Makromol. Chem.* **1965**, *88*, 11.
(3) Burchard, W. *Br. Polym. J.* **1971**, *3*, 214.
(4) Gupta, A. K.; Marchal, E.; Burchard, W. *Macromolecules* **1975**, *8*, 843.
(5) Noordermeer, J. W. M.; Daryanani, R.; Janeschitz-Kriegl, H. *Polymer* **1975**, *16*, 359.
(6) Gupta, A. K.; Cotton, J. P.; Marchal, E.; Burchard, W.; Benoit, H. *Polymer* **1976**, *17*, 363.
(7) Sutter, W.; Burchard, W. *Makromol. Chem.* **1978**, *179*, 1961.
(8) Gupta, A. K.; Marchal, E.; Burchard, W.; Pfannemueller, B. *Macromolecules* **1979**, *12*, 281.
(9) Arnott, S.; Scott, W. E. *J. Chem. Soc., Perkin Trans. 2* **1972**, 324.
(10) Brant, D. A.; Goebel, K. D. *Macromolecules* **1975**, *8*, 522.
(11) Brant, D. A. *Q. Rev. Biophys.* **1976**, *9*, 527.
(12) Zimm, B. H.; Bragg, J. K. *J. Chem. Phys.* **1959**, *31*, 526.
(13) Poland, D. "Cooperative Equilibria in Physical Biochemistry"; Clarendon Press: Oxford, 1978; Chapter 4.
(14) Hayashi, Y.; Teramoto, A.; Kawahara, K.; Fujita, H. *Biopolymers* **1969**, *8*, 403.
(15) Okita, K.; Teramoto, A.; Fujita, H. *Biopolymers* **1970**, *9*, 717.
(16) Goebel, C. V.; Dimpfl, W. L.; Brant, D. A. *Macromolecules* **1970**, *3*, 644.
(17) Goebel, K. D.; Harvie, C. E.; Brant, D. A. *Appl. Polym. Symp.* **1976**, *28*, 671.
(18) Burton, B. A.; Brant, D. A., submitted.
(19) Jordan, R. C.; Brant, D. A.; Cesàro, A. *Biopolymers* **1978**, *17*, 2617.
(20) Brant, D. A.; Burton, B. A. In "Solution Properties of Polysaccharides"; Brant, D. A., Ed.; American Chemical Society: Washington, D.C., 1981, Chapter 7; ACS Symp. Ser. No. 150.
(21) Cook, R.; Moon, M. *Macromolecules* **1980**, *13*, 1537.
(22) Flory, P. J.; Miller, W. G. *J. Mol. Biol.* **1966**, *15*, 284.
(23) Miller, W. G.; Flory, P. J. *J. Mol. Biol.* **1966**, *15*, 298.
(24) Flory, P. J. *Macromolecules* **1974**, *7*, 381.
(25) Brant, D. A.; Dimpfl, W. L. *Macromolecules* **1970**, *3*, 655.
(26) Flory, P. J. "Statistical Mechanics of Chain Molecules"; Wiley-Interscience: New York, 1969; Chapter 4.
(27) Brant, D. A. In "The Biochemistry of Plants"; Preiss, J., Ed.; Academic Press: New York, 1980; Vol. 3, Chapter 11.
(28) Brant, D. A.; Hsu, B., in preparation.
(29) Tanner, D. W.; Berry, G. C. *J. Polym. Sci., Polym. Phys. Ed.* **1974**, *12*, 941.
(30) Kratky, O.; Porod, G. *Recl. Trav. Chim. Pays-Bas* **1949**, *68*, 1106.
(31) Jordan, R. C.; Brant, D. A. *Macromolecules* **1980**, *13*, 491.

Model Calculation of the Conformational Entropy of the High-Pressure Intermediate Phase of Polyethylene

Richard G. Priest

Naval Research Laboratory, Washington, D.C. 20375. *Received January 19, 1982*

ABSTRACT: A model for the high-pressure intermediate phase of polyethylene is outlined. The focus of the model calculation is on the entropy associated with dihedral angle fluctuations of the polymer chain confined by its neighbors to a cylindrical cavity. The constraint of confinement models the intermolecular interactions. Intramolecular interactions are modeled by a conventional dihedral angle potential. An integral equation version of the transfer matrix method is developed in order to analyze the model. In addition to the calculation of the entropy, the formalism allows a calculation of structural properties of the intermediate phase. The correlation with experimental data is discussed.

I. Introduction

The high-pressure intermediate phase of polyethylene, HPIP, has been the subject of a number of experimental investigations.[1] In contrast to the wealth of data, comparatively few theoretical modeling studies have appeared.[2-4] In an earlier paper,[5] I, an integral equation method for the calculation of the entropy of chains confined to cylinders was developed. Such a model is relevant

to the HPIP. The HPIP has been shown to be characterized by extended chains packed into a hexagonal lattice. For this reason it is reasonable to model the structural role of the intermolecular forces by confinement to a cylinder. The basic method used in I is a continuum generalization of the transfer matrix method. Instead of a transfer matrix eigenvalue problem[6] of the form

$$T_{ij}V_j = \lambda V_i \tag{1}$$

an integral equation eigenvalue problem of the form

$$\int K(x,y)V(y)\,dy = \lambda V(x) \tag{2}$$

results.[7] The constraint of confinement to a cylinder is easily expressed in the limits of the integration since the integration is carried out in a cylindrical coordinate system. As in the usual transfer matrix method of analysis, interactions involving nearest-neighbor, second-neighbor, and higher neighbor vertices can be treated. Some applications of the continuum transfer matrix method to related polymer problems have recently appeared.[8-10] The problem relevant to the HPIP is the fixed bond angle chain. For convenience, detailed calculations are carried out with the bond angle set at the tetrahedral value. The constraint of fixed bond length appears as a nearest-neighbor interaction and that of fixed bond angle as a second-neighbor interaction.

The detailed calculations described in I were carried out with a simplified form of the kernel $K(x,y)$. The simplification is valid so long as the radius of the confining cylinder, R, is not too large. The condition is, in effect, that the dihedral angle fluctuation not be larger than about 45° away from the all-trans conformation. This restriction is very severe in light of the goal of modeling the HPIP. Raman spectroscopic studies[11,12] have shown that there are excursions of the dihedral angle into the range of the gauche potential well. To remedy this shortcoming, several improvements have been made in the computational algorithm. These range from the obvious, such as keeping the full expression for the kernal in the integral equation, to more sophisticated computer memory compression strategies. Some of the latter are described in the Appendix.

In addition to avoiding the approximations used in I, it is necessary to take account of the intramolecular dihedral angle potential if large variations of the dihedral angle are to be faithfully modeled. For the purpose of this calculation, it is sufficient to use the Scott–Scheraga, SS, form of this potential.[13] As a function of the dihedral angle α, this potential function has a global minimum at $\alpha = 0$ (trans) and local minima at $\alpha = \pm 120°$ (gauche). Since the positions of four vertices must be given to specify a dihedral angle, the SS potential is a third-neighbor interaction in the sense described above.[13] This presents a practical difficulty because the second-neighbor calculation is near the limit of what can be done in a computer run of reasonable duration. Consequently, an approximate treatment of the SS potential was used. The basis for this approximate treatment is an exact calculation of the a priori four-vertex weights using the nearest-neighbor and second-neighbor interactions. That is, the four-vertex weights are calculated by treating the constraint of fixed bond length and fixed bond angle without approximation. A particular four-vertex weight that can be calculated is the distribution function for the dihedral angle. The approximate treatment of the SS potential is to represent the dihedral angle distribution as a product of two factors. The first factor is the distribution calculated with the nearest-neighbor and second-neighbor interactions but neglect of the SS potential. The second is the distribution calculated by taking only the SS potential into account. This product form may be viewed as a zero-order approximation.

The principal result of this paper is a calculation of the dihedral angle entropy as a function of the cylinder radius R and the temperature T. The temperature dependence arises solely from the SS potential. It is found that there are two local maxima in the entropy with respect to a sloping background as a function of R. The maximum at the lower value of R is associated with the local minimum in the free energy corresponding to the crystal. The maximum at the larger value of R is associated with the local minimum of the free energy corresponding to the HPIP. The largest value of R accessible to the calculation is limited to the value that allows the chain to fold back on itself. It does not appear possible to pursue the calculation to larger values of R and to relax the confinement constraint in such a way as to faithfully model the liquid.

The organization of this paper is as follows. Section II is devoted to the formalism of the integral equation approach. Section III gives the results of the calculations and discusses some of the numerical approximations used. Section IV discusses the results in light of the experimental data on the HPIP. There is an appendix that deals with some of the technical details of the computer algorithm.

II. Formal Development

The method used in this paper and in I is the computation of the partition function, Z, by an integral equation version of the transfer matrix method. Transfer matrix methods are generally applicable to one-dimensional problems. As usually applied to polymers, the one-dimensional topology results because the chains are assumed to have no branching. The problem of a chain confined to a cylinder is one-dimensional because the accessible space is infinite along only one direction. The transfer matrix equations are tractable only if the diameter of the cylinder is small enough to prevent the chain from folding back on itself. The calculations presented here are limited to this case. Since the cylinder is so small, none of the methods of scaling theory are applicable to this problem.

The conformation of a chain of N vertices can be specified by the coordinates of the vertices. The partition function, Z, can be expressed as an integration over these degrees of freedom. This integration can be written in the form

$$Z = \int \prod_i dz_i\, d\vec{\rho}_i\, \delta(|\vec{r}_i - \vec{r}_{i+1}| - 1)\delta(\theta_{i,i+1,i+2} - \theta_b) \tag{3}$$

In this equation the integration is expressed in cylindrical coordinates, which are the natural choice for this problem. The first δ function expresses the constraint that segment length ($|\vec{r}_i - \vec{r}_{i+1}|$) is fixed. The segment length is taken as unity, thus setting the length scale for all the coordinates. The second δ function in eq 3 expresses the constraint of fixed bond angle. The symbol $\theta_{i,i+1,i+2}$ is shorthand notation for the bond angle as a function of $\vec{\rho}_i$, $\vec{\rho}_{i+1}$, and $\vec{\rho}_{i+2}$. In the numerical calculations θ_b is taken as the tetrahedral angle. The constraint of confinement to the cylinder is expressed by restricting the range of integration on $\vec{\rho}_i$ to $\rho_i = |\vec{\rho}_i| < R$, where R is the radius of the cylinder. If there are interactions other than confinement to the cylinder, eq 3 can be suitably augmented.

The δ function enforcing fixed segment length allows the axial degrees of freedom, z_i, to be easily integrated. The result is

$$Z = \int \prod_i d\vec{\rho}_i\, F_{i,i+1}\delta(\theta_{i,i+1,i+2} - \theta_b) \tag{4}$$

with $F_{i,i+1}^{-1} = (1 - \rho_{i,i+1}^2)^{1/2}$ and $\vec{\rho}_{i,i+1} = \vec{\rho}_i - \vec{\rho}_{i+1}$. It is of considerable value to express this in an equivalent form:

$$Z = \int \prod_i d\vec{\rho}_i \, (F_{i,i+1}F_{i+1,i+2})^{1/2} \delta(\theta_{i,i+1,i+2} - \theta_b) \quad (5)$$

The next step is to write the integral equation analogue of the transfer matrix appropriate to eq 5. The derivation of the equation is discussed in I and ref 7. Since eq 5 contains second-neighbor interaction terms, the function acted on by the kernel of the integral equation must be a function of the coordinates of two vertices. The kernel may be read directly from eq 5. The appropriate equation is

$$\int d\vec{\rho}_1 \, d\vec{\rho}_2' \, \hat{K}(\vec{\rho}_1,\vec{\rho}_2';\vec{\rho}_2,\vec{\rho}_3)\phi(\vec{\rho}_1,\vec{\rho}_2') = \lambda\phi(\vec{\rho}_2,\vec{\rho}_3) \quad (6)$$

with

$$\hat{K}(\vec{\rho}_1,\vec{\rho}_2';\vec{\rho}_2,\vec{\rho}_3) = K(\vec{\rho}_1,\vec{\rho}_2,\vec{\rho}_3)\delta(\vec{\rho}_2' - \vec{\rho}_2)$$

$$K(\vec{\rho}_1,\vec{\rho}_2,\vec{\rho}_3) = (F_{1,2}F_{2,3})^{1/2}\delta(\theta_{1,2,3} - \theta_b)$$

The δ function in the expression for $\hat{K}$ reflects the fact that the transfer matrix (here kernel) is zero unless the coordinate that is common to the eigenfunction of the right-hand and left-hand sides of eq 6 has the same value. The integration of $\vec{\rho}_2'$ is immediate, giving the compact form for the eigenequation:

$$\int d\vec{\rho}_1 \, K(\vec{\rho}_1,\vec{\rho}_2,\vec{\rho}_3)\phi(\vec{\rho}_1,\vec{\rho}_2) = \lambda\phi(\vec{\rho}_2,\vec{\rho}_3) \quad (7)$$

It is necessary only to find the solution of eq 7 corresponding to the largest eigenvalue λ_{max}. The a priori weights can be expressed in terms of this eigenfunction. The partition function is given by

$$Z = (\lambda_{max})^N \quad (8)$$

The cylindrical symmetry of the system ensures that $\phi(\vec{\rho}_1,\vec{\rho}_2)$ is actually a function of ρ_1, ρ_2, and θ_{12} as $\phi(\rho_1,\rho_2,\theta_{12})$. Although the integration of $\vec{\rho}_i$ is expressed as a two-dimensional integral, it is essentially one-dimensional by virtue of the δ function in K. That the integration is one-dimensional reflects the fact that there is actually only one true degree of freedom per vertex—the dihedral angle. The integration over ρ_i is converted to a one-dimensional integration according to

$$\int d\vec{\rho}_1 \rightarrow \int d\theta_1 \rho_1 \, G_{1,2,3}$$

$$G_{1,2,3}^{-1} = \left|\frac{\delta}{\delta\rho_1}\theta_{1,2,3}\right| \quad (9)$$

When this is done, ρ_1 is replaced with the value satisfying the δ function in K. The expression for ρ_1 can be easily derived in closed form as a function of θ_{13}, θ_{23}, ρ_2, and ρ_3. It is important, from a practical point of view, that the closed-form solution exists since it represents a considerable savings of computation time. The coordinate system for the integration of eq 7 is shown in Figure 1.

The a priori weight function $W_3(\vec{\rho}_1,\vec{\rho}_2,\vec{\rho}_3)$ can be given in terms of the solution (corresponding to the largest eigenvalue) of eq 7. Averages of functions involving the coordinates of up to three vertices can be calculated by integration over the variables weighted by this function. The form of W_3 for the integral equation approach is exactly analogous to that appropriate to the conventional transfer matrix method.[14] The form is

$$W_3(\vec{\rho}_1,\vec{\rho}_2,\vec{\rho}_3) = \lambda^{-1}\phi(\rho_1,\rho_2,\theta_{12})K(\vec{\rho}_1,\vec{\rho}_2,\vec{\rho}_3)\phi(\rho_3,\rho_2,\theta_{23}) \quad (10)$$

The two-vertex weight functions $W_2(\vec{\rho}_2,\vec{\rho}_3)$ can be obtained from $W_3(\vec{\rho}_1,\vec{\rho}_2,\vec{\rho}_3)$ by integrating with respect to $\vec{\rho}_1$. Using eq 7, we find the result

$$W_2(\vec{\rho}_2,\vec{\rho}_3) = \phi(\rho_2,\rho_3,\theta_{23})\phi(\rho_3,\rho_2,\theta_{23}) \quad (11)$$

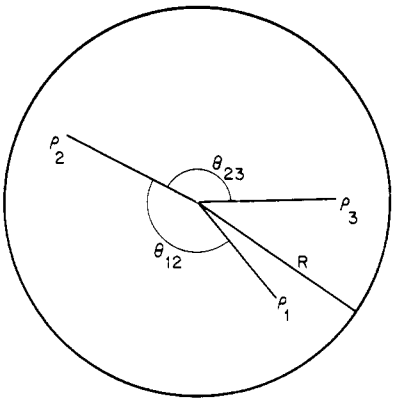

Figure 1. Cylindrical coordinate system used for the solution of eq 7.

This form suggests the normalization condition for ϕ, which is

$$1 = \int d\rho_1 \, d\rho_2 \, \rho_1\rho_2 \, d\theta_{12} \, \phi(\rho_1,\rho_2,\theta_{12})\phi(\rho_2,\rho_1,\theta_{12}) \quad (12)$$

The fairly simple expressions for W_2 and W_3 result partly because of the symmetrical representation of the kernel introduced by eq 5 and 6. If the asymmetrical form of eq 4 is used, a more complex form involving pre- and post-multiplying eigenfunctions results. It is found that the symmetrical form results in a significant savings in computation time.

For the program of calculation outlined in the Introduction it is necessary to calculate four-vertex weight functions. The formalism for doing this can be most easily developed by imagining that there is a four-point interaction to take into account. The appropriate integral equation would then be

$$\int d\rho_1 \, K(\vec{\rho}_1,\vec{\rho}_2,\vec{\rho}_3,\vec{\rho}_4)\phi(\vec{\rho}_1,\vec{\rho}_2,\vec{\rho}_3) = \lambda\phi(\vec{\rho}_2,\vec{\rho}_3,\vec{\rho}_4) \quad (13)$$

with

$$K(\vec{\rho}_1,\vec{\rho}_2,\vec{\rho}_3,\vec{\rho}_4) = [F_{1,2}F_{2,3}^2F_{3,4}]^{1/4}\delta(\theta_{1,2,3} - \theta_b)\delta(\theta_{2,3,4} - \theta_b)V(1,2,3,4)$$

Note that for a four-point interaction ϕ depends on the coordinates of three vertices. Note also that care has been taken to symmetrize the kernel. In the case $V = 1$, i.e., there is no four-point interaction, it is easy to show that

$$\phi(\vec{\rho}_1,\vec{\rho}_2,\vec{\rho}_3) = \lambda^{-1/2}\phi(\vec{\rho}_1,\vec{\rho}_2)[F_{1,2}F_{2,3}]^{1/4}\delta(\theta_{1,2,3} - \theta_b) \quad (14)$$

where $\phi(\vec{\rho}_1,\vec{\rho}_2)$ is the solution to eq 7. The four-point weight function, W_4, can be written down in the same manner as W_3.

$$W_4(\vec{\rho}_1,\vec{\rho}_2,\vec{\rho}_3,\vec{\rho}_4) = \lambda^{-2}\phi(\vec{\rho}_1,\vec{\rho}_2) \times (F_{1,2}F_{2,3})^{1/2}\delta(\theta_{1,2,3} - \theta_b)\delta(\theta_{2,3,4} - \theta_b)(F_{4,3}F_{3,2})^{1/2}\phi(\vec{\rho}_4,\vec{\rho}_3) \quad (15)$$

It is easy to check that

$$\int d\vec{\rho}_1 \, W_4(\vec{\rho}_1,\vec{\rho}_2,\vec{\rho}_3,\vec{\rho}_4) = W_3(\vec{\rho}_2,\vec{\rho}_3,\vec{\rho}_4) \quad (16)$$

The symmetric form of eq 15 is a consequence of the symmetric form of the kernel in eq 6.

A four-vertex function of particular interest is the distribution function for the dihedral angle, $h(\alpha)$. The expression for this function is

$$h(\alpha) = \int d\vec{\rho}_1 \, d\vec{\rho}_2 \, d\vec{\rho}_3 \, d\vec{\rho}_4 \, \delta(\alpha - \alpha(\vec{\rho}_1,\vec{\rho}_2,\vec{\rho}_3,\vec{\rho}_4))W_4(\vec{\rho}_1,\vec{\rho}_2,\vec{\rho}_3,\vec{\rho}_4) \quad (17)$$

The notation $h_0(\alpha)$ will be used for the distribution function when W_4 is calculated from eq 15—that is, in the

approximation of neglecting the four-vertex interaction.

As mentioned above it is not feasible to incorporate four-vertex interactions exactly in these calculations. However, one such interaction, the dihedral angle potential, is allowed by the constraints and is important. For this reason an approximate method of analysis has been developed. The starting point is to represent the dihedral angle potential by the Scott–Scheraga form V_{SS}:

$$V_{SS}(\alpha)/1000k_B\ (\mathrm{K}) = 1.116 + 1.462\cos(\alpha) - 1.578\cos^2(\alpha) - 0.368\cos^3(\alpha) + 3.156\cos^4(\alpha) - 3.788\cos^5(\alpha) \quad (18)$$

As is well-known, the dihedral angle distribution in the absence of the constraint of confinement to the cylinder but under the influence of V_{SS} is

$$h_{SS}(\alpha) = A\exp(-V_{SS}(\alpha)/k_BT) \quad (19)$$

where A is a normalization constant. In these last two equations k_B is Boltzmann's constant. A useful approximate form for $h(\alpha)$ is

$$h(\alpha) = A'h_0(\alpha)h_{SS}(\alpha) \quad (20)$$

This approximate form reduces to the correct expression if either V_{SS} is turned off or the constraint of confinement to a cylinder is removed. In essence, the approximation regards h_0 as arising from a pseudopotential acting on the dihedral angle. The ground for believing that the approximation is a good one is that both $h_0(\alpha)$ and $h_{SS}(\alpha)$ are smooth functions of α.

The final quantity of interest for the purposes of this paper is the entropy, S, associated with the dihedral angle degree of freedom. In principle, this is available from eq 8. However, λ as calculated from eq 5 does not reflect V_{SS}. An approximate method of calculating the entropy that is consistent with regarding h_0 as arising from a pseudopotential is to use the single dihedral angle distribution function.

$$S(T) = -\int h(\alpha)\ln h(\alpha)\,d\alpha \quad (21)$$

This entropy is a function of the temperature, T, through h_{SS}. Equations 7, 9, 15, 17, 20, and 21 form the basis for the numerical calculations of the next section. Together they allow a calculation of S as a function of T for a given value of R.

III. Numerical Results

As indicated in the previous section the first task is to solve eq 7 for λ and ϕ. The basic method used to obtain the numerical solution is the power method. The essence of this method is to choose an initial form of $\phi(\rho_1,\rho_2,\theta_{12})$ and perform the operation indicated on the left-hand side of eq 7. This yields a function that is then, after a suitable normalization, used in the next cycle of iteration. This iterative method is repeated until there is no further change in the form of ϕ. This procedure yields λ_{max} as a byproduct. The rapidity of convergence depends on the ratio of the second largest eigenvalue to λ_{max}. The smaller this ratio, the faster convergence is obtained. For the values of R considered here, about 20 iterations were necessary starting from ϕ = constant. In order to represent $\phi(\rho_1,\rho_2,\theta_{12})$, the kernel, and G numerically, the variables ρ_1, ρ_2, ρ_3, θ_{12}, and θ_{13} were discretized. The angular ranges were divided into 50 intervals and the radial variables into 12. This mesh gave fairly stable results upon slight alteration of the mesh size. Rather than calculate the kernel and G repeatedly, these were tabulated as functions of ρ_2, ρ_3, θ_{12}, and θ_{13}. The dependence on ρ_1 did not need to be separately tabulated since the δ function in K determines ρ_1 once ρ_2, ρ_3, θ_{12}, and θ_{13} are specified. The actual value

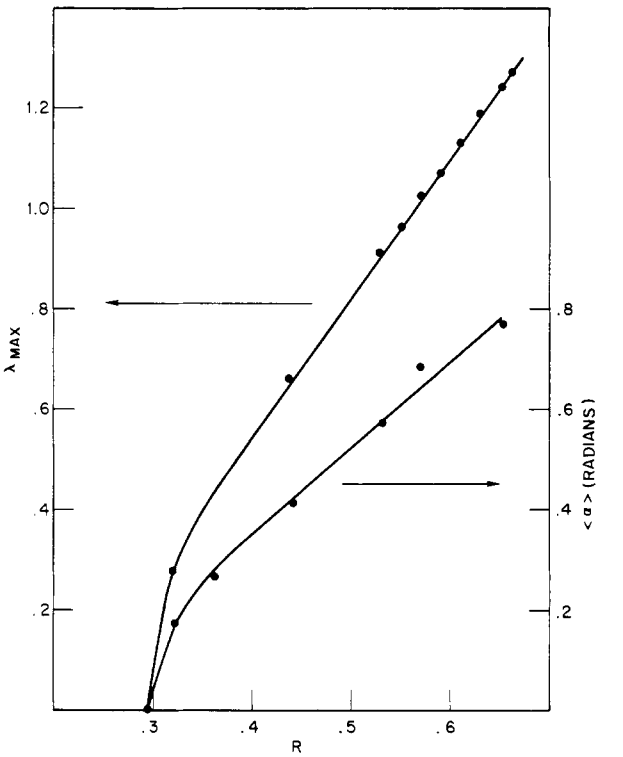

Figure 2. Left-hand scale: Largest eigenvalue of eq 7 for several values of R. Right-hand scale: Average dihedral angle excursion for several values of R. Dihedral angle excursions are always considered positive. In both cases points are calculated and smooth lines are a guide to the eye.

of ρ_1 appropriate to ρ_2, ρ_3, θ_{12}, and θ_{13} was tabulated in a separate table. The fairly large memory requirement for these tables was considerably reduced with the aid of some memory compression techniques discussed in the Appendix. As indicated in eq 9, the integration was generally carried out over θ_1. However, for a limited range of the integrations, G became too large to get accurate results. For these ranges the integration was carried out over ρ_1 instead, with the value of θ_1 fixed by the δ function. The tabular method described above made this switch in integration variable easy to accomplish. The points in the integration range where a switch in integration variable was necessary were encoded in the tables. This technique is discussed further in the Appendix. The result for λ_{max} for various values of R is shown in Figure 2. In this figure, the points were calculated and the curve is intended as a guide to the eye. Each point required approximately 0.75 h of computation time on a DEC10. The remarkable feature of this curve is that for $R > 0.36$ it is indistinguishable from a straight line. This is certainly not an obvious result. To explore the implication of this linearity it is useful to consider the two expressions for the entropy in the case where V_{SS} is neglected. These are

$$S = \ln \lambda_{max} \quad (22)$$

$$S = -\int h_0(\alpha)\ln(h_0(\alpha))\,d\alpha \quad (23)$$

Equation 23 is valid only in the same approximate sense as eq 21. In light of the hard constraint of confinement to the cylinder, it is expected that h_0 is of the form

$$h_0(\alpha) = (1/\alpha_{max})g(\alpha/\alpha_{max}) \qquad |\alpha| < \alpha_{max}$$
$$h_0 = 0 \qquad |\alpha| \geq \alpha_{max} \quad (24)$$

The normalization condition on h_0 forces

$$\int_{-1}^{1} g(y)\,dy = 1 \quad (25)$$

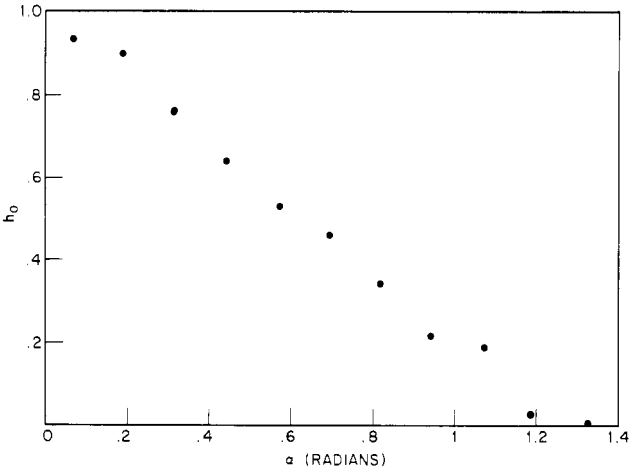

Figure 3. Dihedral angle distribution, h_0, for $R = 0.44$.

Equating the two expressions for the entropy (eq 22 and 23) yields the relation

$$\ln \alpha_{max} - \int_{-1}^{1} g(y) \ln g(y)\, dy = \ln \lambda_{max} \qquad (26)$$

To be consistent with a linear relationship between λ_{max} and R, α_{max} must also be linear in R and the form of $g(y)$ must be independent of R. This is a very strong condition on the form of g. Since $h_0(\alpha)$ can be calculated directly from eq 17, an overall check on the consistency of the calculation and of the approximation of eq 21 is possible.

The results of the numerical calculations of $h_0(\alpha)$ for selected values of R greater than 0.36 confirm the form of eq 22, with α_{max} linear in R. Apart from oscillations originating from the discretization of the variables, the form of g was found to be the same for each value of R.

A typical result for h_0, that for $R = 0.44$, is shown in Figure 3. As is evident from the figure, a good analytic representation of the form of $g(y)$ is $g(y) = 1 - |y|$. A convenient way of summarizing the h_0 calculation is in terms of the average dihedral angle excursion, $\langle\alpha\rangle$. This average was calculated from h_0 as determined from eq 17. The results are shown as the points in Figure 2. Although there is a certain amount of discretization-induced scatter in these values, it is clear that $\langle\alpha\rangle$ and hence α_{max} is a linear function of R for $R > 0.36$. The extrapolation of $\langle\alpha\rangle$ to zero based on the straight line part is at $R \sim 0.2$. This is in agreement with a similar extrapolation for the linear part of the λ_{max} vs. R relationship. This agreement is a further consistency check on the whole calculation. The least-squares linear fit to the linear region gives

$$\langle\alpha\rangle = -0.370 + 1.79R \qquad (27)$$

The final step outlined in the Introduction is the calculation of the entropy, including the Scott–Scheraga potential, via the approximation of eq 20 and 21. The result of this calculation is shown in Figure 4 for four values of the temperature. The zero of the entropy has been set arbitrarily by choosing the discretization interval on α to be 7.2°. In order to obtain the entropy curves as functions of R rather than evaluate S for a discrete set of R values, the analytical form of eq 24 was used for h_0. The dependence of α_{max} on R was taken as $\alpha_{max} = 3\langle\alpha\rangle$, with $\langle\alpha\rangle$ given by eq 27 and $g(y)$ represented by $g(y) = (1 - |y|)$.[15] In addition to allowing calculation as a continuous function of R, this procedure smooths out the numerical oscillations that are the result of the discretization of the variables. These types of small oscillations are evident in Figure 3. They are troublesome because they can obscure the significant features of the curves.

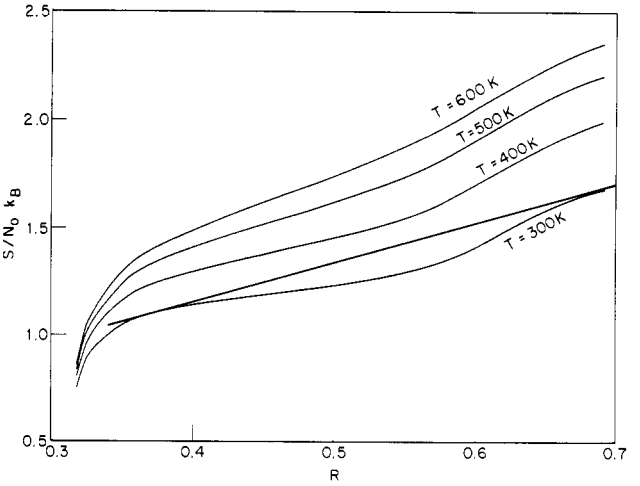

Figure 4. Dihedral angle entropy as a function of R for four values of the absolute temperature. Only entropy differences are significant. Straight line illustrates common-tangent construction.

The most conspicuous feature of the curves in Figure 4 are the two local maxima with respect to a sloping base line. The maximum at the lower value of R (~0.38) results from the rapid increase in the number of accessible chain conformations as R is increased from the minimum value that can accommodate the chain ($R = 0.288$). The maximum that occurs at the larger value of R (~0.68) is the result of the influence of the Scott–Scheraga potential. At about this value of R the value of α_{max} approaches the gauche minimum in V_{SS}. The general method of calculation does not become invalid until $R > 0.785$, at which point the chain can fold back on itself. However, there is a practical limit of $R < {}^2/_3$ imposed by a singularity in the kernel of the integral equation. The singularity is integrable but poses severe numerical difficulties. The simple extrapolation of eq 27, however, allows calculation of S beyond this value. The significance of the two local maxima is discussed in the next section.

IV. Intermediate Phase of Polyethylene

The phase diagram of polyethylene in the T,P plane is marked by the presence of a condensed phase in addition to the melt and orthorhombic crystal phases present at atmospheric pressure. This phase is called the high-pressure intermediate phase. In this section it will be referred to as the intermediate phase, and the orthorhombic phase will be referred to as the crystal phase. The intermediate phase interposes between the crystal and melt in a fairly narrow wedge for pressures and temperatures above the triple point ($P \sim 3.5$ kbar, $T \sim 490$ K). Most of the detailed data have been collected for $P = 5$ kbar. At this pressure the melt–intermediate phase transition is at approximately 526 K and the intermediate–crystal transition is at approximately 519 K.[2] For this reason the interesting region for calculations is $T \sim 500$ K.

The high-pressure intermediate phase of polyethylene is characterized by chain extension and by hexagonal symmetry in the plane normal to the chain extension direction. The accumulated evidence suggests that there is translational disorder along the chain extension direction. These data suggest that a reasonable model for the intermediate state is a fixed bond angle chain confined to a quasi-cylindrical cavity formed by six neighboring chains. In this model all the intermolecular interactions are represented by the constraint of confinement to a cylinder. The sole intramolecular interaction considered is the dihedral angle potential as modeled by V_{SS}. The important degree of freedom in this model from both the thermo-

dynamic and structural point of view is the dihedral angle. The thermodynamic question of interest concerns the amount of entropy associated with the dihedral angle disorder. The structural issue is the amount of shrinkage along the chain extension direction that is caused by the deviations from the all-trans conformation.

The calculation outlined in this paper is parameterized by R, the ratio of the radius of the confining cylinder to the distance between vertices. In order to make a comparison with experimental data it is necessary to make a correspondence between R and a structural parameter of the intermediate phase. In particular, it is desirable to relate R to A, the cross-sectional area of the chain. As formally defined, the confining cylinder confines the chain vertices, which, in the case of polyethylene, coincide with the carbon nuclei. This constraint has its origin in the intermolecular repulsive interactions. However, it is not correct to associate a change in R^2 with a proportional change in A. Such an association is incorrect because neighboring chains have the ability to nest together to some extent, thus leading to a smaller value of A. A detailed analysis of the dependence of A on R would involve chain–chain correlations. While such an analysis is beyond the scope of this paper, a simple argument allows an estimate of A to be made. The argument centers on the value of R that is just large enough to contain the all-trans chain. This value is $R = {}^1/_2 \cos(\theta_b/2)$. If θ_b were to be reduced to θ_b', R would increase to $R' = {}^1/_2 \cos(\theta_b'/2)$. The cross-sectional profile of the chain would elongate somewhat. The cross-sectional area of the chain would increase by an amount, proportional to the elongation, of the order $d_0(R' - R)d_{CC}$, where d_0 is a length on the order of the diameter of the molecular cross section and d_{CC} is the carbon–carbon bond length, 1.54 Å. The factor d_{CC} is needed because of the way R is defined as a dimensionless parameter. An estimate for d_0 can be obtained from the high-pressure data of Bassett et al.[3] The value for $p = 5$ kbar is $d_0 = 5.1$ Å. The appropriate formula for A is then

$$\Delta A = \Delta R d_0 d_{CC} \tag{28}$$

where ΔA is the increase in cross-sectional area due to an increase ΔR in R. For the discussion below this formula will be used to estimate changes in cross-sectional area. Use of this formula is equivalent to an assumption of efficient nesting of neighboring chains.

An examination of Figure 4 shows that there are two interesting values of R, $R \sim 0.38$ and $R \sim 0.68$. These are the two local maxima in S with respect to the sloping base line. The free energy, F, is given by $F = E - TS$. If it is supposed that the internal energy, E, is a quasi-linear increasing function of R for R in the range 0.38–0.68, the free energy will have two local minima with respect to R for some range of temperatures. At a particular temperature the free energy will be identical for the two minima. This is the signature of a first-order phase transition. The transition is between a state characterized by $R \sim 0.38$ and one characterized by $R \sim 0.68$. In the context of the model discussed in the paper the state at $R \sim 0.38$ is identified with the crystal and that at $R \sim 0.68$ with the high-pressure intermediate phase. It is assumed that there is a third minimum in the free energy corresponding to the melt phase at a value of R greater than 0.785. As discussed above, the method of calculation cannot, unfortunately, explore this region. The ground for this assumption is solely that an ordinary melt phase is observed to exist. The schematic form of the free energy as a function of R is shown in Figure 5.

The model does not treat the crystal in a faithful fashion. For this reason the value $R = 0.38$ does not have precise

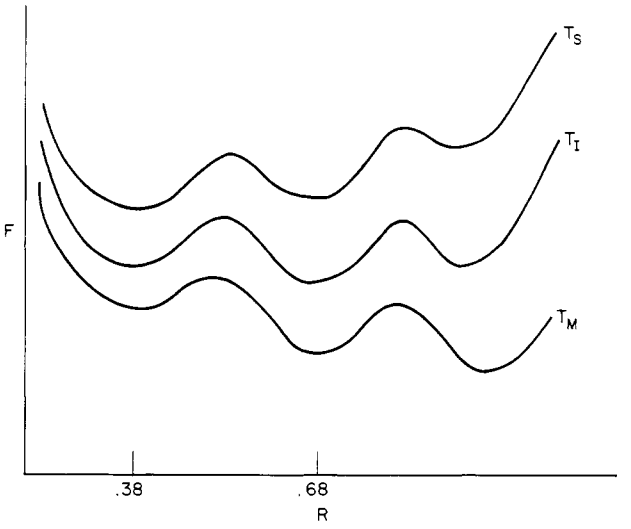

Figure 5. Schematic form of the free energy as a function of R. Part for $R < 0.7$ based on Figure 4. Free energy is shown for three values of the temperature: T_S is a temperature for which the crystal is the stable phase, T_I is a temperature for which the intermediate phase is stable, and T_M is a temperature for which the melt is stable. $T_M > T_I > T_S$.

Table I
Entropy Change at Crystal-Intermediate Phase Transition for Four Temperatures

T, K	$\Delta S/N_0 k_B$
300	0.54
400	0.78
500	0.82
600	0.85

numerical significance. The qualitative feature at $R = 0.38$ does have significance, however. The maximum in the entropy at this value of R represents the entropy of fluctuations restricted to the trans well of the dihedral angle potential. There is a very similar contribution to the entropy in any more refined model of the crystal especially at temperatures of the order 500 K.

The entropy maximum at $R \sim 0.68$ is associated with the intermediate state and not the liquid because the occupation of the gauche well in the dihedral angle potential is only a small fraction of what it is in the melt. Less than 5% of the dihedral angles are in the gauche well at $R = 0.68$. This can be easily seen from Figure 2.

In the absence of knowledge about how the internal energy depends on R, the chief thermodynamic quantity of interest, the transition temperature, cannot be determined. However, the entropy change at the crystal–intermediate phase transition can be estimated. This estimate is the difference between the value of S at the local maximum at $R \sim 0.68$ and its value at $R \sim 0.38$. This entropy difference is presented for four temperatures in Table I. The position of the local maximum can be specified uniquely by the common-tangent procedure illustrated for the case of $T = 300$ K in Figure 4. The experimental value for $T \sim 500$ K is in the range 0.7–0.9 $k_B N_0$ per mole of CH_2.[2] This agreement with the experimental result is very encouraging. It indicates that the entropy maximum at $R \sim 0.68$ is correctly identified with the intermediate phase. An inspection of Table I reveals that the entropy difference increases with increasing temperature. The enthalpy change at the transition between the crystal and intermediate phase, therefore, increases faster than linearly with the temperature. Thus the higher the melting temperature, the more likely is the intermediate phase to be stable. This may be the reason why the

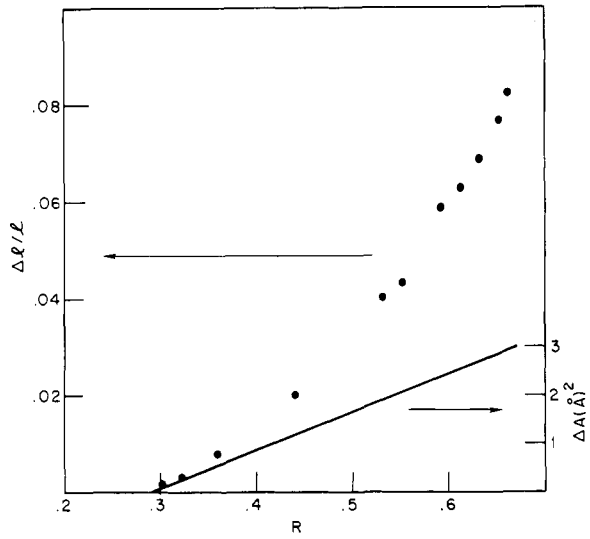

Figure 6. Left-hand scale: Fractional shrinkage in chain length for several values of R. Right-hand scale: Relation between the change in cross-sectional area per chain as a function of R after eq 28.

intermediate phase is stable only at high pressure. It may be simply a result of a higher melting temperature.

In addition to the thermodynamic data, there are two structural data that can be checked against the model. The first is the change in the cross-sectional area per chain at the crystal–intermediate phase transition. According to the thermodynamic interpretation given above, this should be given by eq 28 as $\Delta A = d_0 d_{CC}(0.68 - 0.38)$. This gives $\Delta A = 2.4$ Å^2. This compares fairly well with the experimental value[2] (500 K) of 2.6 Å^2. The second structural datum that can be calculated is the contraction or shrinkage along the chain axis resulting from the large dihedral angle fluctuations. This can be calculated in terms of the fractional shrinkage in the projection of the distance between second-neighbor vertices onto the chain axis.

$$\langle z_{13} \rangle = \left\langle \left(\frac{8}{3}\right)^{1/2} \left(1 - \frac{3}{8}(\rho_1 - \rho_3)^2\right)^{1/2} \right\rangle$$
$$\sim \left(\frac{8}{3}\right)^{1/2} \left(1 - \frac{3}{16}\langle \rho_{13}^2 \rangle\right) \qquad (29)$$

Thus the fractional contraction, $\Delta l/l$, is given by $^3/_{16}\langle \rho_{13}^2 \rangle$. The average $\langle \rho_{13}^2 \rangle$ is readily calculable from W_3. Results for selected R values are given in Figure 6. In this calculation no account of V_{SS} has been taken so there is no temperature dependence. The shrinkage is less than 1% at $R = 0.38$ and on the order of 8% at $R = 0.68$. This latter value compares well with the experimental value for the contraction measured at the crystal–intermediate phase transition. This experimental value for $T = 500$ K is 7%.[2] For convenient reference ΔA as determined from eq 28 is also given in Figure 6.

In conclusion, the model for the high-pressure intermediate phase of polyethylene presented here has four successes. First, the calculation indicates that there is a point of at least local thermodynamic stability for the intermediate phase ($R = 0.68$). Second, a reasonable value for the crystal–intermediate phase entropy discontinuity is obtained. Third, the change in cross-sectional area at the phase transition is correctly obtained. Fourth, the percent shrinkage in chain extension at the phase transition is correctly calculated. These last two predictions are closely related. The model needs to be augmented by an expression for the internal energy as a function of chain cross-sectional area in order for the transition temperature to be calculated. Work is under way to obtain this by molecular mechanics methods.

Acknowledgment. It is a pleasure to thank the Naval Air Systems Command for partial support of this work.

V. Appendix

The solution of eq 7 involves an integration of a δ function in a circular domain. This is equivalent to a line integration in this domain. Both the trajectory of the line and the value of the kernel as a function of position along the line are computationally intensive. The integration must be done repeatedly with the identical form of the kernel and trajectory (for given values of ρ_2, ρ_3, and θ_{23}) but with ϕ varying between cycles. To reduce computational time to a reasonable value, a table look up technique was used. A three-dimensional floating-point array (ρ_1, ρ_2, θ_{12}) was used to store ϕ. The variable θ_{12} was chosen as the integration variable for the line integral. With this choice the trajectory is specified by ρ_1 as a function of ρ_2, ρ_3, θ_{12}, and θ_{23}. The trajectory was stored in a four-dimensional integer array (ρ_2, ρ_3, θ_{12}, θ_{23}) giving the appropriate (discretized) value of ρ_1. The product of the kernel and G was stored in a four-dimensional floating-point array (ρ_2, ρ_3, θ_{12}, θ_{23}). These last two arrays are quite large but need be computed only once.

The array containing ϕ must be resident in random access memory because ρ_1 is a very complex function of the other variables. The two large arrays, however, can be resident on mass storage (disk). The correct organization of the two large arrays on disk is important for the evaluation of four-point weighted averages using W_4 from eq 15. The optimum organization is to choose the index corresponding to θ_{23} as the most slowly varying index. The symmetric form of the kernel allows the same trajectory and kernel arrays to be used for both the ρ_1 and ρ_4 integrations with some permutation of all the indices except the one corresponding to θ_{23}. The four-point weighted averages involve fivefold integration: ρ_2, ρ_3, θ_{12}, θ_{34}, θ_{23}.

The best implementation of the fivefold integration is to choose θ_{23} as the outermost integration. Each time the index corresponding to θ_{23} is changed in the integration routine, a block containing all the elements of the large arrays with the new value of that index is read from the disk into a subarray (three-dimensional) located in random access memory. The subarray occupies a modest amount of memory and allows the index permutation to be done with no additional disk read operations. This implementation causes each element of the large arrays to be read from the disk a single time and provides the best speed–memory size trade-off.

As mentioned above it is desirable to choose θ_{12} as the integration variable for the line integral for most of the integration range. The exceptional case occurs when the trajectory exits the circular domain along a path nearly (or exactly) coinciding with a radius. In this case G becomes very large and the results are numerically unstable. Much better results were obtained in these cases by switching the integration variable to ρ_1. Since the trajectory array is an integer array, it was easy to encode the switching condition by an appropriate modulo arithmetic technique. An appropriate change was made in the large array storing the product of the kernel and G to reflect the modification in G appropriate to integration along ρ_1. The value of θ_{12} does not change appreciably along these trajectory segments so it was not actually necessary to record the value in the arrays. The encoded trajectory array was

used to generate the correct selection from the ϕ array for integration segments of this type.

References and Notes

(1) The most recent review of the properties of this phase is: Leute, U.; Dollhopf, W. *Colloid Polym. Sci.* **1980**, *258*, 353.
(2) Bassett, D. C.; Block, S.; Piermarini, G. *J. Appl. Phys.* **1974**, *45*, 4146.
(3) Bassett, D. C. *Polymer* **1976**, *17*, 460.
(4) Pechhold, W.; Liska, E.; Grossman, H. P.; Hagele, P. C. *Pure Appl. Chem.* **1976**, *46*, 127.
(5) Priest, R. *J. Appl. Phys.* **1981**, *52*, 5930–5933.
(6) The polymer applications of the discrete variable transfer matrix formalism are discussed in: Flory, P. J. "Statistical Mechanics of Chain Molecules"; Interscience: New York, 1969; Chapter III. More recent applications are discussed by Klein (Klein, D. J. *J. Stat. Phys.* **1980**, *23*, 561) and Derrida (Derrida, B. *J. Phys. A* **1981**, *14*, L5).
(7) The essence of the generalization in modern form is found in: Scalapino, D. J.; Sears, M.; Ferrell, R. A. *Phys. Rev. B* **1972**, *6*, 3409. An older reference is: Van Hove, L. *Physica* **1950**, *16*, 137.
(8) Banik, N. C.; Boyle, F. P.; Sluckin, T. J.; Taylor, P. L.; Tripathy, S. K.; Hopfinger, A. J. *Phys. Rev. Lett.* **1979**, *43*, 456–460.
(9) Banik, N. C.; Boyle, F. P.; Sluckin, T. J.; Taylor, P. L.; Tripathy, S. K.; Hopfinger, A. J. *J. Chem. Phys.* **1980**, *72*, 3191–3196.
(10) Banik, N. C.; Taylor, P. L.; Hopfinger, A. J. *Appl. Phys. Lett.* **1980**, *37*, 49–50.
(11) Wunder, S. L. *Macromolecules* **1981**, *14*, 1024–1030.
(12) Tanaka, H.; Takemura, T. *Polym. J.* **1980**, *12*, 349.
(13) Scott, R. A.; Scheraga, H. A. *J. Chem. Phys.* **1966**, *44*, 3054.
(14) Birshtein, T. M.; Pititsyn, O. B. "Conformations of Macromolecules"; Interscience: New York, 1966; Chapter 5.
(15) Note that the relation $\alpha_{max} = 3\langle\alpha\rangle$ follows directly from the form assumed for $g(y)$.

Crystal Structure of Isotactic Poly(methyl methacrylate)

Flip Bosscher,† Gerrit ten Brinke,‡ Arend Eshuis, and Ger Challa*

Laboratory of Polymer Chemistry, State University of Groningen, Nijenborgh 16, 9747 AG Groningen, The Netherlands.

Received November 30, 1981

ABSTRACT: The structure of isotactic poly(methyl methacrylate) (it-PMMA) has been determined by X-ray analysis and energy calculations. X-ray diffraction photographs were taken from an oriented sample of high crystallinity and the intensities and positions of the observed reflections were measured. The results indicate that the unit cell is triclinic although the unit-cell parameters are only slightly different from those of the orthorhombic cells reported in the literature. Favorable conformations are calculated by energy minimization, applying the virtual bond method. Our results support the suggestion of Tadokoro that it-PMMA crystallizes in a double-stranded 10/1 helix with a stabilization energy of 12.4 kJ/(base mol).

Introduction

The structure of isotactic poly(methyl methacrylate) (it-PMMA) is still an open problem, although a considerable number of papers have appeared on this subject. Stroupe and Hughes claimed that their X-ray diffraction patterns could best be interpreted in terms of an orthorhombic unit cell and a 5/2 helical conformation of the backbone.[1] Several studies have appeared since then, using X-ray diffraction[2] and X-ray diffraction combined with energy calculations and infrared spectroscopy.[3,4] All results pointed to a 5/1 helix of the backbone, although different workers suggested different conformations of the side groups. But no one has succeeded in making a complete structural analysis, because of difficulty in indexing the reflections.

A recent communication reported the possibility of a double-stranded 10/1 helix for crystalline it-PMMA.[5] Energy calculations showed this structure to be the more stable one and, furthermore, good packing in a lattice was possible. Other authors objected to this view and considered the single 5/1 helix to be the correct structure,[6] while an examination of the X-ray pattern of it-PMMA in its noncrystalline form showed no evidence that the molecules are paired.[7] So, when double helices were present in crystalline it-PMMA, the chains should pair and intertwine as a part of the crystallization process, which is compatible with the very low rate of crystallization of it-PMMA from the melt.[8] Furthermore, Sundararajan supported the double-stranded helical structure by applying the virtual bond method to it-PMMA, resulting in a more stable 10/1 helix with respect to a 5/1 helix.[9] In this paper we discuss the crystal structure of it-PMMA as determined by X-ray diffraction and energy calculations.

Experimental Section

it-PMMA was prepared from the monomer according to known procedures.[10] The $\bar{M}_v$ of this sample measured in chloroform at 25 °C was 570 000. The tacticity as determined from a 5 wt % *o*-dichlorobenzene solution at 150 °C by 60-MHz NMR spectroscopy was I:H:S = 91:6:3. Uniaxial orientation of the polymer was achieved by stretching a platelet about 300% at 55 °C and subsequently crystallizing it for 3 weeks at 120 °C. The X-ray fiber diagram was recorded photographically with a Statton camera, using Ni-filtered Cu Kα radiation. The intensities of the reflections were measured with an Optronics optical densitometer and stored on magnetic tape. A graphical representation of the intensities along the layer lines was obtained with a digital computer.

Results

The entire fiber diagram and the equatorial reflections are presented in Figures 1 and 2, respectively. Obviously, the reflections are rather diffuse and spread along an arc, as a result of incomplete orientation of the fiber (tangential spread). The intensity along the equator, as determined with the optical densitometer, is given in Figure 3.

When the sample is tilted by 21° with respect to the incident X-rays, the apparent meridional reflection on the fourth layer line (Figure 1) is split into two reflections while a new, really meridional reflection appears on the fifth layer line, indicating a fivefold screw axis. As a matter of

† Present address: Upjohn Polymer B.V., 9930 AD Delfzijl, The Netherlands.
‡ Present address: Polymer Science and Engineering Department, University of Massachusetts, Amherst, MA 01003.

0024-9297/82/2215-1364$01.25/0